Journal of Systems Engineering and Electronics
Vol. 33, No. 1, February 2022, pp.197 – 209

On-line trajectory generation of midcourse cooperative guidance for multiple interceptors

CHEN Wenyu *, SHAO Lei, and LEI Humin

Air and Missile Defense College, Air Force Engineering University, Xi'an 710051, China

Abstract: The cooperative interception trajectories generation of multiple interceptors to hypersonic targets is studied. First, to solve the problem of on-line trajectory generation of the single interceptor, a generation method based on neighborhood optimal control is adopted. Then, when intercepting the strong maneuvering targets, the single interceptor is insufficient in maneuverability, therefore, an on-line multiple trajectories generation algorithm is proposed, which uses the multiple interceptors intercept area (IIA) to cover the target's predicted intercept area (PIA) cooperatively. Through optimizing the interceptors' zero control terminal location, the trajectories are generated on-line by using the neighborhood optimal control method, these trajectories could make the IIA maximally cover the PIA. The simulation results show that the proposed method can greatly improve the interception probability, which provides a reference for the collaborative interception of multiple interceptors.

Keywords: cooperative interception, trajectories generation, near space.

DOI: 10.23919/JSEE.2022.000020

1. Introduction

The hypersonic vehicle is a weapon that can fly continuously in the near space at five times of the speed of sound. Compared with the traditional ballistic missile, it has a variable trajectory, strong maneuverability in a wide scope and a high speed. The vehicle brings great pressure to the existing air defense system. Therefore, it is urgent to develop interception technology for hypersonic vehicles. Many scholars have studied the interception of hypersonic targets in the near space, including the tracking and prediction of target trajectory, and the generation and tracking of interceptor trajectory. For the generation of interceptor trajectory, the current mainstream idea is to generate an off-line trajectory according to the interceptor initial state and the target state before the launch of the interceptor. This trajectory usually guarantees one best performance index, which makes the interceptor launch to the best interceptor position in the terminal guidance. However, the target usually does not adopt the fixed flight mode, and will carry out a series of strong maneuvers. The original terminal constraints are no longer applicable, so a new optimal trajectory needs to be generated on-line. On-line trajectory generation must be completed in a short time. Because the offline optimal generation method needs a relatively long time, and the method is no longer applicable, it is necessary to select an on-line fast optimization method, and generate an on-line trajectory based on the original offline trajectory. The on-line trajectory must meet the changed terminal states. In addition, a single interceptor often fails to intercept the target because of its lack of maneuverability. Therefore, in order to increase the success rate of interception, we should pay more attention to the way that multiple interceptors intercept the target cooperatively.

In view of the on-line generation of correction trajectory, there are few existing researches dedicated to the near space interceptor. However, many scholars have carried out research on similar issues, which brings a lot of references for the on-line generation of trajectory of near space interceptors. With the characteristics of high efficiency and rapidity of the model predictive static programming algorithm, Dwivedi et al. studied the problem of trajectory optimization [1−4]. Although the problem is mainly aimed at trajectory optimization, the essence of trajectory on-line generation and correction of the interceptor is also an optimization problem, and it just needs a more rapid solution. Therefore, the method also has a reference significance. Although the method can consider process constraints, it cannot guarantee the optimality of the index function. In [5−7], the problem of orbit correction of the lunar exploration vehicle is solved by using the theory of variable neighborhood optimal control, and the correction of control quantity under the change of the terminal constraint is solved. However, it is mainly aimed

Manuscript received June 23, 2020.
*Corresponding author.
This work was supported by the National Natural Science Foundation of China (61873278).

at the situation of the change of the remaining flight time, which is not consistent with the background of the interceptor. In [8] and [9], the neighborhood optimal control method and the pseudospectral method were combined to solve the correction of the control quantity. However, only for the situation where initial states change, it cannot fulfill the situation that the terminal constraint changes on-line. Williams et al. studied the trajectory optimization of spacecraft and the design of the optimal guidance law [10−12]. Zhou et al. also applied the neighborhood optimal control method to study trajectory optimization, generation and tracking of the middle guidance phase, all of which took some explorations for the on-line generation of interceptor trajectory [13−18].

The cooperative interception problem of multiple interceptors stems from the inspiration of unmanned aerial vehicle (UAV) cooperative search technology, and scholars pay more and more attention to it based on the cooperative theory. In [19], to solve the problem of multiple interceptors intercepting multiple targets through optimizing the performance index, which is maximizing the probability that multiple interceptors intercept multiple targets, good results were achieved. In [20], the uncertainty of target trajectory states prediction was considered, and the terminal area of the target was described by the probability density distribution function. The reachable area of the interceptor can maximize the coverage of the possible area of the target. The linearization assumption of the motion model was made in [21], the intercepted area of the interceptor was analyzed by the true proportional guidance method, and a new cooperative strategy was proposed. Ma et al. studied the problem of multiple interceptors cooperating in intercepting high-speed targets in the longitudinal plane [22−24]. The cooperative method of multiple interceptors is derived. There is no research on cooperative multiple interceptors in the middle guidance stage.

In this paper, to achieve the maximum coverage of the target's predicted intercept area (PIA) by the interceptor's intercept area (IIA), through optimizing the terminal position of multiple interceptors, the trajectories of multiple interceptors are generated on-line. Based on the existing standard trajectories, the trajectories are generated on-line with the neighborhood optimal control method. Based on direct force correction of interceptors in the terminal guidance stage, the IIA is deduced, and the terminal positions of multiple interceptors are optimized. The terminal positions of multiple interceptors are fully optimized by the on-line generation method, so as to achieve the maximum coverage of the target's PIA by the IIA. The simulation results show that when the target maneuvers and the PIA changes longitudinally and laterally, the method in this paper can achieve the cooperative coverage of the PIA with a high coverage rate.

2. On-line trajectory generation algorithm of single interceptor

The neighborhood optimization algorithm is developed from optimal control [25]. Firstly, suppose that the motion differential equation of the interceptor in longitudinal plane [26] is

$$\begin{cases} \dot{V} = \dfrac{(P\cos\alpha - C_D qs)}{m} - g\sin\Theta \\ \dot{\Theta} = \dfrac{(P\sin\alpha + C_L qs)}{mV} - \left(\dfrac{g}{V} - \dfrac{V}{R_0 + h}\right)\cos\Theta \\ \dot{h} = V\sin\Theta \\ \dot{L} = \dfrac{R_0 V\cos\Theta}{R_0 + h} \end{cases} \tag{1}$$

where V is the interceptor velocity, Θ is the velocity path angle, h is the height, L is the range, P is the engine thrust, the attack angle α is the control variable, m is the mass; C_L and C_D are the lift coefficient and drag coefficient respectively, s is the reference area, q is the dynamic pressure, and R_0 is the average radius of the earth. The equation could be shown as

$$\dot{\boldsymbol{x}} = \boldsymbol{f}(\boldsymbol{x}, \boldsymbol{u}, t) \tag{2}$$

where $\boldsymbol{f}$ describes the motion law of the interceptor, $\boldsymbol{x}$ is the state vector, $\boldsymbol{u}$ is the control vector, and t is a free variable. All derivatives in this paper are derivatives of time.

The performance index function is

$$J = \phi(\boldsymbol{x}(t_f), t_f) + \int_{t_0}^{t_f} L(\boldsymbol{x}, \boldsymbol{u}, t)\mathrm{d}t = -\boldsymbol{V}_f \tag{3}$$

where ϕ is the terminal quantity, t_0 is the initial time, t_f is the terminal time, L is the Lagrange function, and $\boldsymbol{V}_f$ is the interceptor terminal velocity.

The terminal constraint is

$$\boldsymbol{\psi}(\boldsymbol{x}(t_f), t_f) = [h(t_f) - h_f \quad \Theta(t_f) - \Theta_f]^{\mathrm{T}} = \boldsymbol{0} \tag{4}$$

where h_f and Θ_f are the terminal height and velocity path angle. The Hamiltonian function is

$$H = L(\boldsymbol{x}, \boldsymbol{u}, t) + \boldsymbol{\lambda}^{\mathrm{T}} \boldsymbol{f}. \tag{5}$$

By using the Lagrange multiple plier method, the equality constraints and terminal constraints are introduced into the index function:

$$J' = \phi(\boldsymbol{x}(t_f), t_f) + \boldsymbol{v}^{\mathrm{T}} \boldsymbol{\psi}(\boldsymbol{x}(t_f), t_f) + \int_{t_0}^{t_f} \left(H - \boldsymbol{\lambda}^{\mathrm{T}} \dot{\boldsymbol{x}}\right)\mathrm{d}t \tag{6}$$

where $\boldsymbol{\lambda} \in \mathbf{R}^n$ is the Lagrange multiple plier vector, and $\boldsymbol{v} \in \mathbf{R}^q$ is the Lagrange multiple plier. When the control quantity is unconstrained, to maximize the functional index J, the necessary condition should satisfy:

(i) State equation and co-state equation

$$\begin{cases} \dot{\boldsymbol{x}} = \dfrac{\partial H}{\partial \boldsymbol{\lambda}} \\ \dot{\boldsymbol{\lambda}} = -\dfrac{\partial H}{\partial \boldsymbol{x}} \end{cases} \tag{7}$$

(ii) Boundary and cross section conditions

$$\begin{cases} \boldsymbol{x}(t_0) = \boldsymbol{x}_0 \\ \boldsymbol{\psi}(\boldsymbol{x}(t_f), t_f) = \boldsymbol{0} \\ \boldsymbol{\lambda}(t_f) = \left[\dfrac{\partial \phi}{\partial \boldsymbol{x}} + \dfrac{\partial \boldsymbol{\psi}^{\mathrm{T}}}{\partial \boldsymbol{x}}\boldsymbol{v}\right]_{t=t_f} \end{cases} \tag{8}$$

(iii) Coupling condition

$$\frac{\partial H}{\partial \boldsymbol{u}} = \boldsymbol{0} \tag{9}$$

(iv) When t_f is free, the Hamiltonian function satisfies

$$\left[H + \frac{\partial \phi}{\partial t} + \boldsymbol{v}^{\mathrm{T}}\frac{\partial \boldsymbol{\psi}}{\partial t}\right]_{t=t_f} = 0. \tag{10}$$

The above equations are the necessary conditions for the function to satisfy the first-order optimality. When satisfying the first-order optimality, the system has a small disturbance and initial state $\boldsymbol{x}(t_0)$ or terminal constraint $\boldsymbol{\psi}_f$ changes, the deviation of the state variable on the reference trajectory $\delta\boldsymbol{x}(t)$ is

$$\delta\boldsymbol{x}(t) = \boldsymbol{x}(t) - \boldsymbol{x}^*(t) \tag{11}$$

where $\boldsymbol{x}^*(t)$ represents the value along the optimal trajectory. $\boldsymbol{x}(t)$ represents the filtered data after the actual measurement. In order to maintain the optimal trajectory, the deviation of the optimal control quantity is

$$\delta\boldsymbol{u}(t) = \boldsymbol{u}(t) - \boldsymbol{u}^*(t) \tag{12}$$

where $\boldsymbol{u}^*(t)$ represents the optimal control variable. The first-order optimality condition formulae (7)−(10) are obtained by taking the following variations [27].

$$\delta\dot{\boldsymbol{x}} = \frac{\partial^2 H}{\partial\boldsymbol{\lambda}\partial\boldsymbol{x}}\delta\boldsymbol{x} + \frac{\partial^2 H}{\partial\boldsymbol{\lambda}\partial\boldsymbol{u}}\delta\boldsymbol{u} \tag{13}$$

$$\delta\dot{\boldsymbol{\lambda}} = -\frac{\partial^2 H}{\partial\boldsymbol{x}^2}\delta\boldsymbol{x} - \frac{\partial^2 H}{\partial\boldsymbol{x}\partial\boldsymbol{\lambda}}\delta\boldsymbol{\lambda} - \frac{\partial^2 H}{\partial\boldsymbol{x}\partial\boldsymbol{u}}\delta\boldsymbol{u} \tag{14}$$

$$\frac{\partial^2 H}{\partial\boldsymbol{u}\partial\boldsymbol{x}}\delta\boldsymbol{x} + \frac{\partial^2 H}{\partial\boldsymbol{u}\partial\boldsymbol{\lambda}}\delta\boldsymbol{\lambda} + \frac{\partial^2 H}{\partial\boldsymbol{u}^2}\delta\boldsymbol{u} = 0 \tag{15}$$

$$\delta\boldsymbol{x}(t_0) = \delta\boldsymbol{x}_0 \tag{16}$$

$$\left[\frac{\partial\boldsymbol{\psi}}{\partial\boldsymbol{x}}\delta\boldsymbol{x} + \left(\frac{\partial\boldsymbol{\psi}}{\partial\boldsymbol{x}}\frac{\mathrm{d}\boldsymbol{x}}{\mathrm{d}t} + \frac{\partial\boldsymbol{\psi}}{\partial t}\right)\mathrm{d}t_f\right]_{t=t_f} = \mathrm{d}\boldsymbol{\psi}_f \tag{17}$$

$$\left[\left(\frac{\partial\boldsymbol{\lambda}}{\partial\boldsymbol{\lambda}}\right)\delta\boldsymbol{\lambda} + \frac{\partial\boldsymbol{\lambda}}{\partial t}\mathrm{d}t_f\right]_{t=t_f} = \left[\frac{\partial^2\boldsymbol{\Phi}}{\partial\boldsymbol{x}^2}\delta\boldsymbol{x} + \frac{\partial\boldsymbol{\psi}^{\mathrm{T}}}{\partial\boldsymbol{x}}\mathrm{d}\boldsymbol{v} + \frac{\mathrm{d}}{\mathrm{d}t}\left(\frac{\partial\boldsymbol{\Phi}}{\partial\boldsymbol{x}}\right)\mathrm{d}t_f\right]_{t=t_f} \tag{18}$$

$$\left[\left(\frac{\partial H}{\partial\boldsymbol{\lambda}}\right)^{\mathrm{T}}\delta\boldsymbol{\lambda} + \left(\frac{\partial H}{\partial\boldsymbol{x}} + \frac{\partial^2\boldsymbol{\Phi}}{\partial\boldsymbol{x}\partial t}\right)\delta\boldsymbol{x} + \frac{\partial\boldsymbol{\psi}^{\mathrm{T}}}{\partial t}\mathrm{d}\boldsymbol{v} + \left(\frac{\partial H}{\partial t} + \frac{\mathrm{d}}{\mathrm{d}t}\left(\frac{\partial\boldsymbol{\Phi}}{\partial t}\right)\right)\mathrm{d}t_f\right]_{t=t_f} = 0 \tag{19}$$

Among them, $\boldsymbol{\Phi} = \phi(\boldsymbol{x}(t_f), t_f) + \boldsymbol{v}^{\mathrm{T}}\boldsymbol{\psi}(\boldsymbol{x}(t_f), t_f)$. The above conditions are to make the performance index J optimal when the initial state $\boldsymbol{x}(t_0)$ or terminal constraints change by $\mathrm{d}\boldsymbol{\psi}_f$. Related principles could be known in [28]. The above conditions are second-order optimal. There is a second-order approach between the trajectory satisfying the second-order optimal condition and the real optimal trajectory, based on which, the calculation method of the neighborhood optimization algorithm based on second-order variation is deduced. From (15),

$$\delta\boldsymbol{u} = -\left(\frac{\partial^2 H}{\partial\boldsymbol{u}^2}\right)^{-1}\frac{\partial^2 H}{\partial\boldsymbol{u}\partial\boldsymbol{x}}\delta\boldsymbol{x} - \left(\frac{\partial^2 H}{\partial\boldsymbol{u}^2}\right)^{-1}\frac{\partial^2 H}{\partial\boldsymbol{u}\partial\boldsymbol{\lambda}}\delta\boldsymbol{\lambda}. \tag{20}$$

Taking (20) into (13) and (14), there are

$$\begin{cases} \delta\dot{\boldsymbol{x}} = \left(\dfrac{\partial^2 H}{\partial\boldsymbol{\lambda}\partial\boldsymbol{x}} - \dfrac{\partial^2 H}{\partial\boldsymbol{\lambda}\partial\boldsymbol{u}}\left(\dfrac{\partial^2 H}{\partial\boldsymbol{u}^2}\right)^{-1}\dfrac{\partial^2 H}{\partial\boldsymbol{u}\partial\boldsymbol{x}}\right)\delta\boldsymbol{x} - \\ \qquad \dfrac{\partial^2 H}{\partial\boldsymbol{\lambda}\partial\boldsymbol{u}}\left(\dfrac{\partial^2 H}{\partial\boldsymbol{u}^2}\right)^{-1}\dfrac{\partial^2 H}{\partial\boldsymbol{u}\partial\boldsymbol{\lambda}}\delta\boldsymbol{\lambda} \\ \delta\dot{\boldsymbol{\lambda}} = \left(-\dfrac{\partial^2 H}{\partial\boldsymbol{x}^2} + \dfrac{\partial^2 H}{\partial\boldsymbol{x}\partial\boldsymbol{u}}\left(\dfrac{\partial^2 H}{\partial\boldsymbol{u}^2}\right)^{-1}\dfrac{\partial^2 H}{\partial\boldsymbol{u}\partial\boldsymbol{x}}\right)\delta\boldsymbol{x} + \\ \qquad \left(\dfrac{\partial^2 H}{\partial\boldsymbol{x}\partial\boldsymbol{u}}\left(\dfrac{\partial^2 H}{\partial\boldsymbol{u}^2}\right)^{-1}\dfrac{\partial^2 H}{\partial\boldsymbol{u}\partial\boldsymbol{\lambda}} - \dfrac{\partial^2 H}{\partial\boldsymbol{x}\partial\boldsymbol{\lambda}}\right)\delta\boldsymbol{\lambda} \end{cases} \tag{21}$$

where $\delta\boldsymbol{X}(t) = \begin{bmatrix} \delta\boldsymbol{x}(t) \\ \delta\boldsymbol{\lambda}(t) \end{bmatrix}$, then

$$\delta\dot{\boldsymbol{X}} = \begin{bmatrix} \delta\dot{\boldsymbol{x}} \\ \delta\dot{\boldsymbol{\lambda}} \end{bmatrix} = \begin{bmatrix} \boldsymbol{C}_1(t) & \boldsymbol{C}_2(t) \\ \boldsymbol{C}_3(t) & -\boldsymbol{C}_1^{\mathrm{T}}(t) \end{bmatrix}\begin{bmatrix} \delta\boldsymbol{x} \\ \delta\boldsymbol{\lambda} \end{bmatrix} = \boldsymbol{C}\delta\boldsymbol{X}. \tag{22}$$

where

$$\begin{cases} \boldsymbol{C}_1(t) = \left[\dfrac{\partial^2 H}{\partial\boldsymbol{\lambda}\partial\boldsymbol{x}} - \dfrac{\partial^2 H}{\partial\boldsymbol{\lambda}\partial\boldsymbol{u}}\left(\dfrac{\partial^2 H}{\partial\boldsymbol{u}^2}\right)^{-1}\dfrac{\partial^2 H}{\partial\boldsymbol{u}\partial\boldsymbol{x}}\right] \\ \boldsymbol{C}_2(t) = \left[-\dfrac{\partial^2 H}{\partial\boldsymbol{\lambda}\partial\boldsymbol{u}}\left(\dfrac{\partial^2 H}{\partial\boldsymbol{u}^2}\right)^{-1}\dfrac{\partial^2 H}{\partial\boldsymbol{u}\partial\boldsymbol{\lambda}}\right] \\ \boldsymbol{C}_3(t) = \left[-\dfrac{\partial^2 H}{\partial\boldsymbol{x}^2} + \dfrac{\partial^2 H}{\partial\boldsymbol{x}\partial\boldsymbol{u}}\left(\dfrac{\partial^2 H}{\partial\boldsymbol{u}^2}\right)^{-1}\dfrac{\partial^2 H}{\partial\boldsymbol{u}\partial\boldsymbol{x}}\right] \end{cases}. \tag{23}$$

Assuming that $\delta\boldsymbol{X}(t_f)$ is known, we can calculate the inverse recurrence integral of (22):

$$\delta\boldsymbol{X}(t_{k-1}) = \delta\boldsymbol{X}(t_k) + \boldsymbol{C}(t_k)\delta\boldsymbol{X}(t_k)\Delta t = (\boldsymbol{E}_{n\times n} + \boldsymbol{C}(t_k)\Delta t)\delta\boldsymbol{X}(t_k). \tag{24}$$

where $\Delta t = -\mathrm{d}t$, $\delta\boldsymbol{X}(t_k) = \delta\boldsymbol{X}(t_f)$. Similarly,

$$\delta \boldsymbol{X}(t_{k-2}) = \delta \boldsymbol{X}(t_{k-1}) + \boldsymbol{C}(t_{k-1})\delta \boldsymbol{X}(t_{k-1})\Delta t = (\boldsymbol{E}_{n\times n} + \boldsymbol{C}(t_{k-1})\Delta t)\delta \boldsymbol{X}(t_{k-1}) = (\boldsymbol{E}_{n\times n} + \boldsymbol{C}(t_{k-1})\Delta t)(\boldsymbol{E}_{n\times n} + \boldsymbol{C}(t_k)\Delta t)\delta \boldsymbol{X}(t_k). \tag{25}$$

It can be obtained by recursion in turn:

$$\delta \boldsymbol{X}(t_0) = \boldsymbol{C}_F \delta \boldsymbol{X}(t_k),$$

$$\boldsymbol{C}_F = (\boldsymbol{E}_{n\times n} + \boldsymbol{C}(t_1)\Delta t)(\boldsymbol{E}_{n\times n} + \boldsymbol{C}(t_2)\Delta t)\cdots(\boldsymbol{E}_{n\times n} + \boldsymbol{C}(t_k)\Delta t). \tag{26}$$

If the first-order optimality condition of the optimal control problem has been solved, $\boldsymbol{u}^*(t)$ and $\boldsymbol{x}^*(t)$ of (7)−(10) are satisfied, then the coefficients in (17)−(19) can be solved along the optimal trajectory, and can be sorted into the following linear equations:

$$\mathrm{d}\boldsymbol{\psi}_f = \left[\frac{\partial \boldsymbol{\psi}}{\partial \boldsymbol{x}}\delta \boldsymbol{x} + \left(\frac{\partial \boldsymbol{\psi}}{\partial \boldsymbol{x}}\frac{\mathrm{d}\boldsymbol{x}}{\mathrm{d}t} + \frac{\partial \boldsymbol{\psi}}{\partial t}\right)\mathrm{d}t_f\right]_{t=t_f}, \tag{27}$$

$$\left[-\frac{\partial^2 \boldsymbol{\Phi}}{\partial \boldsymbol{x}^2}\delta \boldsymbol{x} + \delta \boldsymbol{\lambda}\right]_{t=t_f} + \left[\frac{\partial \boldsymbol{\lambda}}{\partial t} - \frac{\mathrm{d}}{\mathrm{d}t}\left(\frac{\partial \boldsymbol{\Phi}}{\partial \boldsymbol{x}}\right)\right]_{t=t_f}\mathrm{d}t_f = \left(\frac{\partial \boldsymbol{\psi}^{\mathrm{T}}}{\partial \boldsymbol{x}}\right)_{t=t_f}\mathrm{d}\boldsymbol{v}, \tag{28}$$

$$\left[\left(\frac{\partial H}{\partial \boldsymbol{x}} + \frac{\partial^2 \boldsymbol{\Phi}}{\partial \boldsymbol{x}\partial t}\right)\delta \boldsymbol{x} + \left(\frac{\partial H}{\partial \boldsymbol{\lambda}}\right)^{\mathrm{T}}\delta \boldsymbol{\lambda} + \left(\frac{\partial H}{\partial t} + \frac{\mathrm{d}}{\mathrm{d}t}\left(\frac{\partial \boldsymbol{\Phi}}{\partial t}\right)\right)\mathrm{d}t_f\right]_{t=t_f} = -\left(\frac{\partial \boldsymbol{\psi}^{\mathrm{T}}}{\partial \boldsymbol{x}}\right)_{t=t_f}\mathrm{d}\boldsymbol{v}. \tag{29}$$

In the linear equations system composed of (26)−(28), there are a total of $2n+q+1$ unknowns, which are n dimensions variable $\delta \boldsymbol{x}$, n dimensions variable $\delta \boldsymbol{\lambda}$, q dimensions variable $\mathrm{d}\boldsymbol{v}$ and one dimension variable $\mathrm{d}t_f$. However, there are only $n+q+1$ equations. According to the structural theorem of the solution of the linear equation system, there must be n free variables in $2n+q+1$ variables. Take the variable on the right side of (27)−(29) as a free variable and record it as a vector $\mathrm{d}\boldsymbol{\mu}$ [29], then

$$\mathrm{d}\boldsymbol{\mu}^{\mathrm{T}} = [\mathrm{d}v_1, \mathrm{d}v_2, \mathrm{d}v_3, \cdots, \mathrm{d}v_q, \delta x_{q+1}, \delta x_{q+2}, \cdots, \delta x_n]_{t=t_f} \tag{30}$$

where $\delta x_{q+1}, \delta x_{q+2}, \cdots, \delta x_n$ are the variable $\delta \boldsymbol{x}$ without terminal constraints, which cannot be solved by (27). If the equations of (27) and (28) are linearly independent, it can be solved

$$\begin{bmatrix} \delta \boldsymbol{X}(t_f) \\ \mathrm{d}t_f \end{bmatrix} = \begin{bmatrix} \delta \boldsymbol{x} \\ \delta \boldsymbol{\lambda} \\ \mathrm{d}t_f \end{bmatrix}_{t=t_f} = \begin{bmatrix} \boldsymbol{F}_{11} & \boldsymbol{F}_{12} \\ \boldsymbol{F}_{21} & \boldsymbol{F}_{22} \\ \boldsymbol{F}_{31} & \boldsymbol{F}_{32} \end{bmatrix}\begin{bmatrix} \mathrm{d}\boldsymbol{\mu} \\ \mathrm{d}\boldsymbol{\psi}_f \end{bmatrix}. \tag{31}$$

When $t_k = t_f$, by taking (31) into (26), we can get

$$\delta \boldsymbol{X}(t_0) = \boldsymbol{C}_F \begin{bmatrix} \boldsymbol{F}_{11} & \boldsymbol{F}_{12} \\ \boldsymbol{F}_{21} & \boldsymbol{F}_{22} \end{bmatrix}\begin{bmatrix} \mathrm{d}\boldsymbol{\mu} \\ \mathrm{d}\boldsymbol{\psi}_f \end{bmatrix}. \tag{32}$$

Let $\boldsymbol{CF}$ be

$$\boldsymbol{CF} = \begin{pmatrix} \boldsymbol{CF}_{11} & \boldsymbol{CF}_{12} \\ \boldsymbol{CF}_{21} & \boldsymbol{CF}_{22} \end{pmatrix} = \begin{pmatrix} \boldsymbol{C}_F(1:n, 1:n) & \boldsymbol{C}_F(1:n, n+1:2n) \\ \boldsymbol{C}_F(n+1:2n, 1:n) & \boldsymbol{C}_F(n+1:2n, n+1:2n) \end{pmatrix}\begin{pmatrix} \boldsymbol{F}_{11} & \boldsymbol{F}_{12} \\ \boldsymbol{F}_{21} & \boldsymbol{F}_{22} \end{pmatrix}.$$

where $1:n$ means the elements from 1 to n. Then

$$\begin{cases} \boldsymbol{CF}_{11} = \boldsymbol{C}_F(1:n, 1:n)\boldsymbol{F}_{11} + \boldsymbol{C}_F(1:n, n+1:2n)\boldsymbol{F}_{21} \\ \boldsymbol{CF}_{12} = \boldsymbol{C}_F(1:n, 1:n)\boldsymbol{F}_{12} + \boldsymbol{C}_F(1:n, n+1:2n)\boldsymbol{F}_{22} \\ \boldsymbol{CF}_{21} = \boldsymbol{C}_F(n+1:2n, 1:n)\boldsymbol{F}_{11} + \boldsymbol{C}_F(n+1:2n, n+1:2n)\boldsymbol{F}_{21} \\ \boldsymbol{CF}_{22} = \boldsymbol{C}_F(n+1:2n, 1:n)\boldsymbol{F}_{12} + \boldsymbol{C}_F(n+1:2n, n+1:2n)\boldsymbol{F}_{22} \\ \boldsymbol{F}_{11} = \boldsymbol{F}(1:n, 1:n) \\ \boldsymbol{F}_{12} = \boldsymbol{F}(1:n, n+1:n+q) \\ \boldsymbol{F}_{21} = \boldsymbol{F}(n+1:2n, 1:n) \\ \boldsymbol{F}_{22} = \boldsymbol{F}(n+1:2n, , n+1:n+q) \end{cases}.$$

Then (32) can be written as

$$\delta \boldsymbol{X}(t_0) = \begin{pmatrix} \delta \boldsymbol{x}(t_0) \\ \delta \boldsymbol{\lambda}(t_0) \end{pmatrix} = \begin{pmatrix} \boldsymbol{CF}_{11} & \boldsymbol{CF}_{12} \\ \boldsymbol{CF}_{21} & \boldsymbol{CF}_{22} \end{pmatrix}\begin{pmatrix} \mathrm{d}\boldsymbol{\mu} \\ \mathrm{d}\boldsymbol{\psi}_f \end{pmatrix}. \tag{33}$$

Therefore,

$$\begin{cases} \delta \boldsymbol{x}(t_0) = \boldsymbol{CF}_{11}\mathrm{d}\boldsymbol{\mu} + \boldsymbol{CF}_{12}\mathrm{d}\boldsymbol{\psi}_f \\ \delta \boldsymbol{\lambda}(t_0) = \boldsymbol{CF}_{21}\mathrm{d}\boldsymbol{\mu} + \boldsymbol{CF}_{22}\mathrm{d}\boldsymbol{\psi}_f \end{cases}. \tag{34}$$

From the above formulae,

$$\begin{cases} \delta \boldsymbol{x}(t_m) = \boldsymbol{CF}_{11}(t_m)\mathrm{d}\boldsymbol{\mu} + \boldsymbol{CF}_{12}(t_m)\mathrm{d}\boldsymbol{\psi}_f \\ \delta \boldsymbol{\lambda}(t_m) = \boldsymbol{CF}_{21}(t_m)\mathrm{d}\boldsymbol{\mu} + \boldsymbol{CF}_{22}(t_m)\mathrm{d}\boldsymbol{\psi}_f \end{cases} \tag{35}$$

where $t_m \in [t_0, t_f]$. If $\boldsymbol{CF}_{11}$ is reversible, then

$$\mathrm{d}\boldsymbol{\mu} = \boldsymbol{CF}_{11}^{-1}(\delta \boldsymbol{x}(t_0) - \boldsymbol{CF}_{12}\mathrm{d}\boldsymbol{\psi}_f). \tag{36}$$

Take (35) and (36) into (20) to get

$$\delta \boldsymbol{u}(t_m) = -\left(\frac{\partial^2 H}{\partial \boldsymbol{u}^2}\right)^{-1}\frac{\partial^2 H}{\partial \boldsymbol{u}\partial \boldsymbol{x}}\delta \boldsymbol{x}(t_m) - \left(\frac{\partial^2 H}{\partial \boldsymbol{u}^2}\right)^{-1}\frac{\partial^2 H}{\partial \boldsymbol{u}\partial \boldsymbol{\lambda}}\delta \boldsymbol{\lambda}(t_m) = \left[-\left(\frac{\partial^2 H}{\partial \boldsymbol{u}^2}\right)^{-1}\frac{\partial^2 H}{\partial \boldsymbol{u}\partial \boldsymbol{x}} - \left(\frac{\partial^2 H}{\partial \boldsymbol{u}^2}\right)^{-1}\frac{\partial^2 H}{\partial \boldsymbol{u}\partial \boldsymbol{\lambda}}\boldsymbol{CF}_{21}(t_m)\boldsymbol{CF}_{11}^{-1}(t_m)\right]\delta \boldsymbol{x}(t_m) - \left(\frac{\partial^2 H}{\partial \boldsymbol{u}^2}\right)^{-1}\frac{\partial^2 H}{\partial \boldsymbol{u}\partial \boldsymbol{\lambda}}\left(\boldsymbol{CF}_{22}(t_m) - \boldsymbol{CF}_{21}(t_m)\boldsymbol{CF}_{11}^{-1}(t_m)\boldsymbol{CF}_{12}(t_m)\right)\mathrm{d}\boldsymbol{\psi}_f. \tag{37}$$

That means the adjustment variable of the reference control variable can be expressed by the current state deviation $\delta \boldsymbol{x}(t_m)$ and the terminal constraint adjustment

variable $\mathrm{d}\boldsymbol{\psi}_f$. Assume that

$$\begin{cases} \boldsymbol{U}_x(t_m) = -\left(\dfrac{\partial^2 H}{\partial \boldsymbol{u}^2}\right)^{-1} \dfrac{\partial^2 H}{\partial \boldsymbol{u}\partial \boldsymbol{x}} - \\ \quad \left(\dfrac{\partial^2 H}{\partial \boldsymbol{u}^2}\right)^{-1} \dfrac{\partial^2 H}{\partial \boldsymbol{u}\partial \boldsymbol{\lambda}} \boldsymbol{CF}_{21}(t_m)\boldsymbol{CF}_{11}^{-1}(t_m) \\ \boldsymbol{U}_\psi(t_m) = -\left(\dfrac{\partial^2 H}{\partial \boldsymbol{u}^2}\right)^{-1} \dfrac{\partial^2 H}{\partial \boldsymbol{u}\partial \boldsymbol{\lambda}} \cdot \\ \quad \left(\boldsymbol{CF}_{22}(t_m) - \boldsymbol{CF}_{21}(t_m)\boldsymbol{CF}_{11}^{-1}(t_m)\boldsymbol{CF}_{12}(t_m)\right) \end{cases} . \quad (38)$$

In this paper, only the case of terminal constraints change is involved. Therefore, the on-line generation of interceptor trajectory caused by the change of state quantity is not considered. Therefore, $\delta \boldsymbol{x}(t_m) = 0$. When the target is maneuvering, only the end constraints of the interceptor reference trajectory are changed. Based on the original reference optimal trajectory, the following control adjustments need to be generated:

$$\delta \boldsymbol{u}(t_m) = -\left(\frac{\partial^2 H}{\partial \boldsymbol{u}^2}\right)^{-1} \frac{\partial^2 H}{\partial \boldsymbol{u}\partial \boldsymbol{\lambda}} \left(\boldsymbol{CF}_{22}(t_m) - \boldsymbol{CF}_{21}(t_m)\boldsymbol{CF}_{11}^{-1}(t_m)\boldsymbol{CF}_{12}(t_m)\right) \mathrm{d}\boldsymbol{\psi}_f = \boldsymbol{U}_\psi(t_m)\mathrm{d}\boldsymbol{\psi}_f . \quad (39)$$

According to (39), the block diagram of neighborhood optimal control applied to trajectory on-line generation is drawn as shown in Fig. 1.

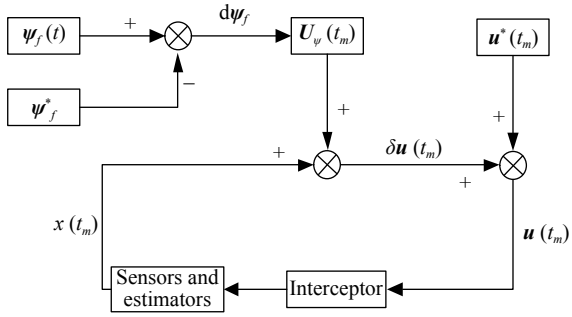

Fig. 1 On-line trajectory generation block diagram

In order to verify the ability of on-line trajectory generation of the interceptor under the neighborhood optimal control method, the following simulation experiments are carried out. First of all, the initial height of the interceptor is 60 km, the initial velocity is 4 000 m/s, the initial angle of reentry is −4°, the terminal height required for the standard trajectory is 30 km, and the terminal angle is 0°. With the actual situation considered, when the terminal constraints are changed due to the target's maneuvering, and with the assumption that the terminal height changes to 28 km, the corresponding simulation figures are as follows in Fig. 2−Fig. 5. In Fig. 2, H is the flight height, and L is the flight length of the interceptor.

From the simulation, it can be seen that for the scenario where the terminal conditions of the reference trajectory are changing, the trajectory on-line generation under the neighborhood optimal control can find a trajectory satisfying the terminal constraints.

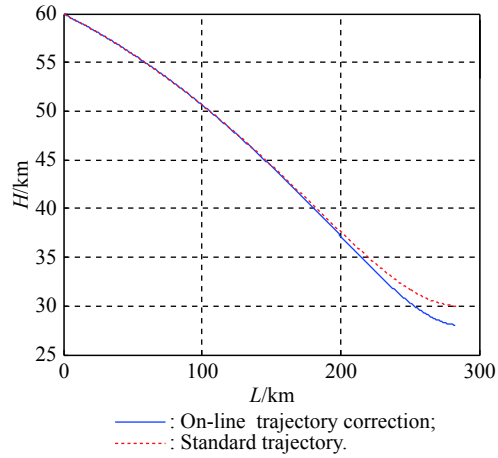

Fig. 2 Trajectories in longitudinal plane

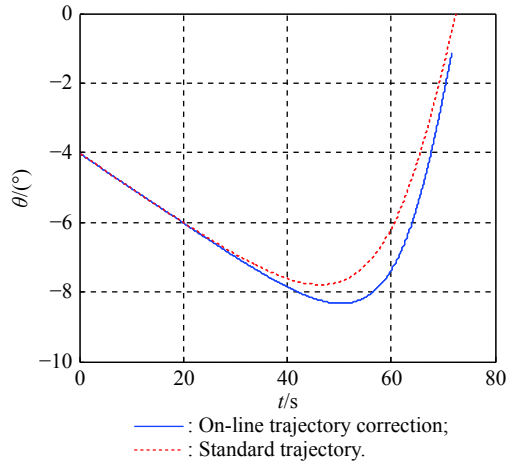

Fig. 3 Change of ballistic inclination

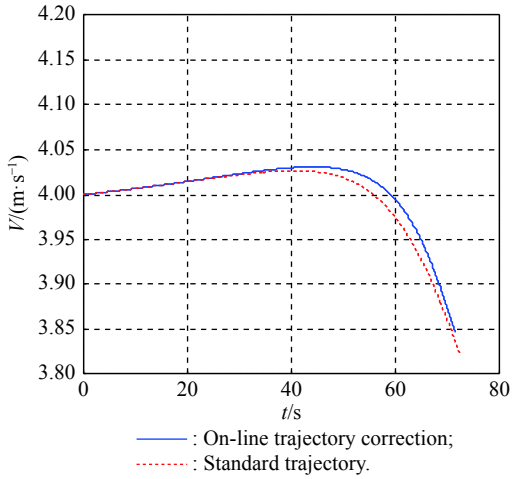

Fig. 4 Change of flight speed

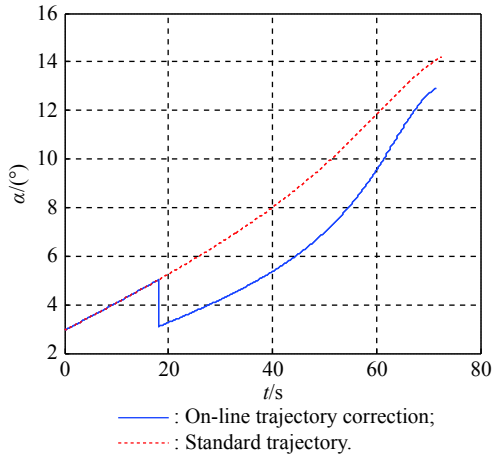

Fig. 5 Change of attack angle

The above simulation is only for the scenario where the position constraints change. In order to verify the universality of the method and the correction ability of interceptors for different PIAs, carry out 50 Monte Carlo simulations, keep the above initial conditions unchanged, and generate the terminal position randomly within 5 km based on the original standard trajectory. The simulation results are as follows in Fig. 6−Fig. 10.

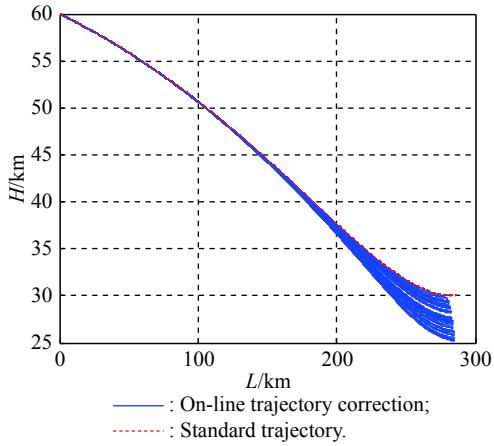

Fig. 6 Trajectories in longitudinal plane under 50 simulations

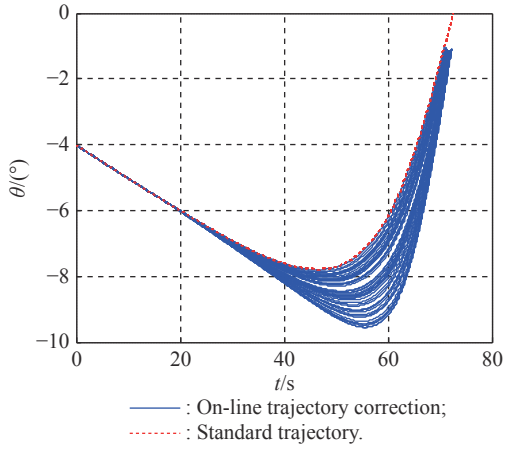

Fig. 7 Change of ballistic inclination under 50 simulations

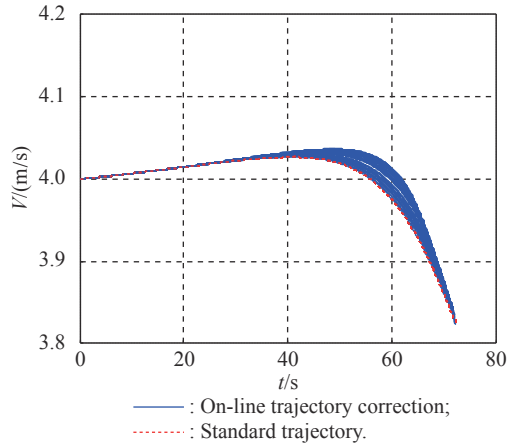

Fig. 8 Change of flight speed under 50 simulations

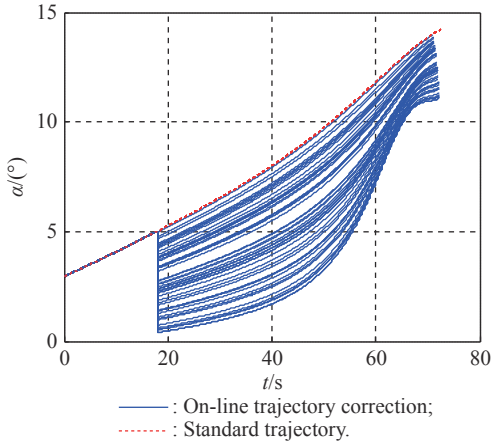

Fig. 9 Change of attack angle under 50 simulations

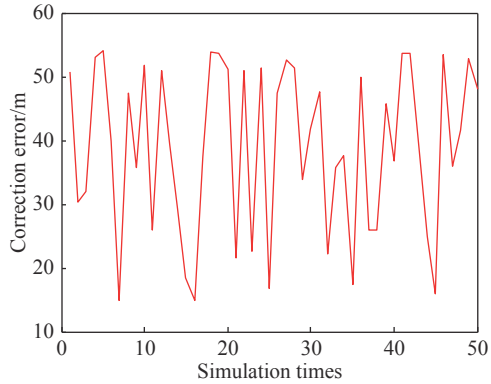

Fig. 10 Terminal error of on-line trajectories generation under 50 simulations

According to Fig. 10, the error between the on-line corrected terminal position and the expected terminal position is within 55 m, which can well meet the terminal constraints. Because the miss distance is not the most important index of the terminal constraint of midcourse guidance, the above error can meet the midcourse and terminal shift of midcourse guidance of the interceptor completely,

and it can be corrected in the terminal guidance. It is proved that the on-line correction method of neighborhood optimal control used in this paper can complete the on-line trajectory generation of the interceptor. However, it can be seen in the figure that when the terminal constraint is modified, the required control variable of the interceptor will jump to a certain extent, which means that the control variable of the interceptor will change dramatically. The maneuverability of a single interceptor is required to be high. Therefore, this paper proposes to use multiple interceptors to complete the mission.

3. On-line trajectories generation of multiple interceptors

3.1 Multiple interceptors' IIA cooperatively covering the PIA

Definition 1 PIA: the set of all possible location points of the target at the time t_{f1} of prediction hit is called PIA, which is recorded as R. Therefore, the area where the predicted hit probability exists can be expressed [30] as

$$R = \{\boldsymbol{X} | \boldsymbol{X} \sim N(\boldsymbol{X}(t_{f1}, \boldsymbol{P}(t_{f1}))\}. \tag{40}$$

where $\boldsymbol{P}(t_{f1})$ is the covariance matrix of the prediction intercept area.

By projecting PIA and IIA into the missile target encounter plane, the coverage of PIA in three-dimensional space can be transformed into the area coverage in plane, as shown in Fig. 11.

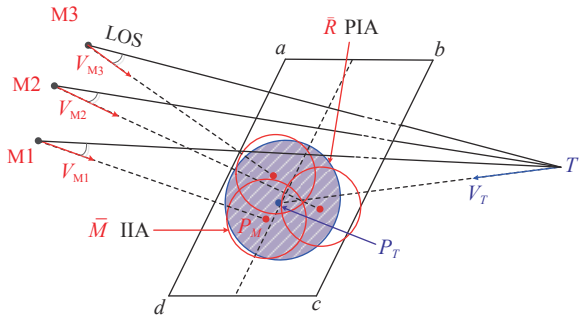

Fig. 11 PIA of target and IIA of multiple interceptors

In Fig. 11, M and T represent the interceptor and the target respectively, P_M is the zero control terminal position of the interceptor, plane a-b-c-d is the encounter plane of the missile and the target, where P_T is the projection of the mean point of PIA in plane, $\bar{R}$ and $\bar{M}$ are the projections of PIA and IIA in plane respectively. After projection, the IIA and target PIA can be expressed as

$$\bar{M} = \{(y,z) | |y - y_d| \leqslant S_{\max}, |z - z_d| \leqslant S_{\max}\} \tag{41}$$

where $S_{\max}$ is the maximum correction distance, (x_d, y_d, z_d) is the zero control terminal position.

$$\bar{R} = \{(y,z) | (y,z) \sim N(\boldsymbol{X}_1(t_{f1}), \boldsymbol{P}_1(t_{f1}))\} \tag{42}$$

In order to intercept the target, the interceptor needs to be overloaded about three times of the target's maneuver value. It is undeniable that interceptors are inferior in hypersonic targets maneuver. To ensure the interceptor successfully intercepts the target, it is necessary to ensure that the IIA completely covers the PIA. From the above simulations, it can be seen that the trajectory generated online by a single interceptor can meet the changed terminal constraints after the change of the terminal constraints of the satndard trajectory, but the control variable will inevitably change dramatically. This shows that under the condition of overload limitation, a single interceptor is difficult to complete effective interception. However, if multiple interceptors are used to intercept cooperatively, and the IIA is used to cover the PIA after target's maneuver, the probability of successful interception will be greatly improved.

3.2 Mathematical description of cooperative coverage problem

Interceptors are regarded as agents in the collaborative process. N agents need to cover the target area $R \in \mathbf{R}^2$, the location set of all agents is $P = \{p_1, p_2, \cdots, p_N\}$. Let $\boldsymbol{p}_i = [p_i^y, p_i^z]^{\mathrm{T}}$ represents agent A_i in the target area, the probability density distribution function of the target area is $\phi(\xi) : R \to \mathbf{R}^+$, where $\xi \in R$ represents any point in the target area R. In order to describe the coverage effect of multiple agents quantitatively, let $h(\boldsymbol{p}_i, \xi)$ represent the cost function of agent A_i covering the point ξ:

$$h(\boldsymbol{p}_i, \xi) = \|\boldsymbol{p}_i - \xi\|. \tag{43}$$

Therefore, the coverage cost function of multiple agents to the target area can be expressed as

$$H(P, R, \phi) = \int_R h(\boldsymbol{p}_i, \xi)\phi(\xi)\mathrm{d}\xi. \tag{44}$$

Formula (44) is the location optimization function. From (44), we can see that each agent has the ability to cover the points $\xi \in R$ in the target area. The greater distance from the point ξ to the agent, the greater cost to cover the point, and the worse coverage performance. In order to make the cost function in the area covering problem $H(P, R, \phi)$ minimum, select the agent with the smallest distance to cover the point. Therefore, by optimizing the location of multiple agents and adjusting the allocation area of each agent, the cost function could be minimized. Based on the Voronoi segmentation principle, the above statement is proved as follows:

Theorem 1 In the target area $R \in \mathbf{R}^2$, N agents are randomly distributed, and their location information is P. According to the location information of the current time, the optimal region segmentation principle of multiple agents cooperative coverage is Voronoi segmentation.

Proof In order to minimize the coverage cost function. There is

$$H(P,R,\phi)=\int_R \min_{i\in\{1,\cdots,n\}} h(\boldsymbol{p}_i,\xi)\phi(\xi)\mathrm{d}\xi. \tag{45}$$

The minimum distance from the point ξ to N agents is

$$D_\xi=\min_{i\in\{1,\cdots,n\}} h(\boldsymbol{p}_i,\xi). \tag{46}$$

According to the minimum distance, the target area can be divided into N independent sub areas, in which the set of the closest points to the agent can be expressed as

$$R_i=\{\xi\in R|h(p_i,\xi)\leqslant h(\boldsymbol{p}_j,\xi),\forall j\neq i,\forall i,j\in N\}. \tag{47}$$

where R_i is the sub area to be covered by the agent A_i, $R=\{R_1,R_2,\cdots,R_N\}$ represents the sub area of each agent. The optimal covering cost function of the corresponding agents to the target area is

$$H_1(P,R,\phi)=\sum_{i=1}^{N}\int_{R_i} h(\boldsymbol{p}_i,\xi)\phi(\xi)\mathrm{d}\xi. \tag{48}$$

According to this lemma, in the target area, the optimal coverage area of each agent is the Voronoi area. □

3.3 Optimization of multiple interceptors' zero control terminal location

3.3.1 Modeling of IIA with energy constraints

It is assumed that the aerodynamic control is used in the midcourse guidance and the direct force control is used in the final guide. The aerodynamic correction ability is obviously affected by the altitude of the interceptor, and the direct lateral force correction ability is limited by the energy carried.

In the final guidance, it is assumed that the maximum working time of the orbit control engine is $t_{\max}$, the specific impulse of the orbit control engine is I_g, the maximum steady-state thrust is $P_{\max}$, and the initial mass of the interceptor terminal guidance is m_{m0}. If the interceptor is always propelled by the maximum steady-state thrust, the mass change rate of the interceptor is

$$\dot{m}=-\frac{P_{\max}}{I_g g}. \tag{49}$$

The interceptor's maximum lateral acceleration at time t can be expressed as follows:

$$a_{\max}(t)=\frac{P_{\max}}{m_{m0}+\dot{m}t}=\frac{P_{\max}}{m_{m0}-\dfrac{P_{\max}}{I_g g}t}. \tag{50}$$

According to (50), the lateral velocity and the maximum lateral maneuver displacement of the interceptor at time t can be calculated as follows:

$$v(t)=\int_0^t a_{\max}(\tau)\mathrm{d}\tau, \tag{51}$$

$$S_m=\int_0^t\int_0^t a_{\max}(\tau)\mathrm{d}\tau\mathrm{d}t. \tag{52}$$

From the beginning of the terminal guidance time t_h to the interception time t_f, if $(t_f-t_h)\leqslant t_{\max}$, the maximum lateral displacement of the interceptor perpendicular to the initial velocity vector direction is

$$S_{\max}=\int_0^{t_{f1}-t_f}\int_0^{t_{f1}-t_f} a_{\max}(\tau)\mathrm{d}\tau\mathrm{d}t. \tag{53}$$

If $(t_f-t_h)\geqslant t_{\max}$,

$$S_{\max}=\int_0^{t_{\max}}\int_0^{t_{\max}} a_{\max}(\tau)\mathrm{d}\tau\mathrm{d}t \tag{54}$$

under the condition of direct force and energy limitation, the IIA in the terminal guidance stage of the interceptor is determined by $S_{\max}$. The IIA of the interceptor can be expressed as

$$M(t_h)=\{(x,y,z)||y-y_d|\leqslant S_{\max},|z-z_d|\leqslant S_{\max}\}. \tag{55}$$

Among them, the IIA depends on the working time of the direct force device in the terminal guidance stage.

In order to ensure that the interceptor successfully intercepts the target at the final time, it is necessary to ensure that the IIA can completely cover the PIA at the hand-off time

$$R(t_f)\subseteq M(t_f) \tag{56}$$

where $R(t_f)$ represents the PIA.

3.3.2 Optimal solution of multiple interceptors' zero control terminal position

At the hand-off time, the projection of the PIA in the encounter plane of the missile is $\bar{R}$, there is the point $(y,z)\in\bar{R}$, and the lateral coordinate of the interceptor M_i zero control terminal position at the end of the shift is (y_i,z_i), then the zero control miss distance of the interceptor M_i relative to the point (y,z) is

$$Z_i=\sqrt{(y_i-y)^2+(z_i-z)^2}. \tag{57}$$

There is a zero control miss distance between point (y,z) and each interceptor, and the minimum one is chosen as the zero control miss distance between point (y,z) and N interceptors.

$$Z = \min_{i=1,\cdots,n} \sqrt{(y_i - y)^2 + (z_i - z)^2} \tag{58}$$

The mathematical expectation of zero control miss distance of N interceptors at the hand-off time is

$$E_1 = \iint_{\bar{R}} \min_{i=1,\cdots,n} \sqrt{(y_i - y)^2 + (z_i - z)^2} f_k(y)\mathrm{d}y f_k(z)\mathrm{d}z. \tag{59}$$

where $f_k(y)$ and $f_k(z)$ are the probability density functions of the target at y axis and z axis. The estimated value of the target position obeys normal distribution, the mathematical expectation of target position at y axis and z axis is $[\mu_y \ \mu_z]$, and the variance is $[\sigma_y \ \sigma_z]$. There are

$$\begin{cases} f_k(y) = \dfrac{1}{\sqrt{2\pi}\sigma_y} \exp\left(-\dfrac{(x-\mu_y)^2}{2\sigma_y^2}\right) \\ f_k(z) = \dfrac{1}{\sqrt{2\pi}\sigma_z} \exp\left(-\dfrac{(z-\mu_z)^2}{2\sigma_z^2}\right) \end{cases}. \tag{60}$$

$p_1(y,y_i)p_1(z,z_i)$ is the cost function of coverage, which could judge whether the point (y,z) is within the interceptor's intercepting capability, there are

$$p_1(y,y_i) = \begin{cases} 1, & |y - y_i| \leqslant S_{\max} \\ 0, & |y - y_i| > S_{\max} \end{cases}, \tag{61}$$

$$p_1(z,z_i) = \begin{cases} 1, & |z - z_i| \leqslant S_{\max} \\ 0, & |z - z_i| > S_{\max} \end{cases}. \tag{62}$$

According to the probability distribution function of the target at the hand-off time, the probability of the target appearing in the IIA is

$$H_2 = \int_{\bar{R}} (p_1(y,y_i)p_1(z,z_i)) f_k(y)\mathrm{d}y f_k(z)\mathrm{d}z. \tag{63}$$

When the flight overload of the interceptor is certain, at the hand-off time, H_2 depends on the position, speed direction, and sight angle of the interceptor. If the interceptor's overload is enough, the interceptor's IIA can completely cover the PIA of the target, so that $H_2 = 1$. To determine whether the point (y,z) is in IIA of N interceptors, the coverage performance function is

$$p_2 = 1 - \prod_{i=1}^{n} (1 - p_1(y,y_i)p_1(z,z_i)). \tag{64}$$

If $p_2 = 1$, it means that there is an interceptor satisfying $p_1(y,y_i)p_1(z,z_i) = 1$, and that means the point (y,z) is in the IIA. According to the probability distribution function of the target, the probability that the target appears in the IIA of N interceptors is

$$H_3 = \iint_{\bar{R}} \left(1 - \prod_{i=1}^{n} (1 - p_1(y,y_i)p_1(z,z_i))\right) f_k(y)\mathrm{d}y f_k(z)\mathrm{d}z. \tag{65}$$

At the hand-off time, in order to maximize the performance of multiple interceptors' IIA coverage, it is necessary to control the status of the interceptors midcourse guidance terminal through the midcourse guidance trajectory on-line generation technology, so as to control the zero control terminal positions of the interceptors. Assuming that the number of interceptors meets the requirements, $P_{\min}$ is the cooperative coverage requirement, the problem can be described as

$$\begin{cases} E_1 = \iint_{\bar{R}} \min_{i=1,\cdots,n} \sqrt{(y_i - y)^2 + (z_i - z)^2} f_k(y)\mathrm{d}y f_k(z)\mathrm{d}z \\ \text{s.t. } H_3(n,(y_1,z_1),\cdots,(y_n,z_n)) \geqslant P_{\min} \end{cases}. \tag{66}$$

By solving the optimization problem (66), the number required and the optimal zero control terminal position of multiple interceptors can be obtained, and then the optimal medium guidance terminal state constraint of multiple interceptors can be obtained.

According to the Voronoi segmentation method of the region, the set of the closest point to the interceptor M_i can be

$$\bar{R}_i = \left\{(y,z) \in R \middle| \sqrt{(y_i - y)^2 + (z_i - z)^2} \leqslant \sqrt{(y_j - y)^2 + (z_j - z)^2}, \forall i \neq j, \forall i, j \in \{1,\cdots,n\}\right\} \tag{67}$$

where $\bar{R}_i$ is the sub-region to be covered by the interceptors M_i interceptable region.

Then (59) can be described as

$$E_1 = \sum_{i=1}^{n} \iint_{\bar{R}_i} \sqrt{(y_i - y)^2 + (z_i - z)^2} f_k(y)\mathrm{d}y f_k(z)\mathrm{d}z. \tag{68}$$

In order to simplify the problem, suppose that the adjustment of the interceptor terminal position at y axis and z axis is independent of each other, (68) can be rewritten as

$$E_1 = \sum_{i=1}^{n} \iint_{\bar{R}_i} (|y_i - y| + |z_i - z|) f_k(y)\mathrm{d}y f_k(z)\mathrm{d}z. \tag{69}$$

If

$$\begin{cases} E_{1y} = \displaystyle\sum_{i=1}^{n} \int_{\bar{R}_i} |y_i - y| f_k(y)\mathrm{d}y \\ E_{1z} = \displaystyle\sum_{i=1}^{n} \int_{\bar{R}_i} |z_i - z| f_k(z)\mathrm{d}z \end{cases}, \tag{70}$$

then we can get

$$E_1 = E_{1y} + E_{1z}. \tag{71}$$

By using the optimality condition, the optimal zero control terminal position can be obtained by optimizing E_{1y} and E_{1z}.

Based on the above, the specific solution steps of the on-line trajectories generation of cooperative multiple interceptors are as follows:

Step 1 At the hand-off time, by using the target trajectory prediction algorithm, the target motion information detected by multiple-source sensors is used to get the probability density function of the target position, and the PIA of the target is obtained.

Step 2 With the advance of the interception task, the prediction time of the target becomes shorter and the PIA converges gradually. According to the change of PIA, under the constraint of the cooperative coverage performance index of IIA, the optimal zero control terminal position of multiple interceptors is calculated, and the zero control terminal position is transformed into the terminal position constraint of guidance in each interceptor.

Step 3 Under the new terminal state constraints, each interceptor uses the neighborhood optimal control trajectory on-line generation algorithm to generate the control instruction correction variable on-line, so as to adjust the terminal position of the interceptor trajectory and realize the control of zero control terminal position of the interceptor; if the generated terminal condition cannot be executed, it needs to return to Step 2.

Step 4 Determine whether the cooperative coverage condition is met. If so, repeat Step 1; if not, go to Step 2.

4. Simulation analysis

In order to verify the effectiveness of the guidance trajectories generation method for the cooperative coverage of the IIA, the following two scenarios are simulated. The simulation assumes that the maximum operating distance of the interceptor terminal guidance is 100 km, and the terminal guidance time is taken as $t_f = 20$ s; the maximum correction distance of the rail control engine working for 20 s is taken as $S_{\max} = 5$ km; the probability density function distribution of the PIA follows the normal distribution.

Scenario 1: It mainly verifies the capability of on-line trajectory generation of multiple interceptors after the longitudinal change of the PIA. By using the IIA of four interceptors to cover the PIA, the PIA at the end of the middle guidance stage is obtained by predicting the target trajectory,

$$\bar{R}_1 = \{(y,z)|9\,392.9 \leqslant y \leqslant 37\,677.1,$$
$$24\,392.9 \leqslant z \leqslant 52\,677.1, \sigma_y = \sigma_z = 4\,714\}.$$

Assuming that the target measurement information is updated once in the 30 s of midcourse guidance, the PIA after the update is

$$\bar{R}_2 = \{(y,z)|16\,463.9 \leqslant y \leqslant 30\,606.1,$$
$$26\,463.9 \leqslant z \leqslant 40\,606.1, \sigma_y = \sigma_z = 2\,357\}.$$

The initial conditions of the base trajectories of the four interceptors are set as follows in Table 1.

Table 1 Initial condition setting of medium guidance reference trajectory

V_0/(m/s)	x_0/km	y_0/km	θ_0/(°)	ψ_{v0}/(°)
3 000	0	80	−3	0

Among them, the initial positions of M1, M2, M3 and M4 are 10 km, 20 km, 27.07 km and 37.07 km respectively. According to the PIA, the terminal state of the interceptor can be optimized as in Table 2 and Table 3.

Table 2 Terminal condition setting of medium guidance reference trajectory

Missile	V_f/(m/s)	x_f/km	y_f/km	z_f/km	θ_f/(°)	ψ_{vf}/(°)
M1	Max	600	20	42.07	0	0
M2	Max	600	20	35	0	0
M3	Max	600	27.07	35	0	0
M4	Max	600	27.07	42.07	0	0

Table 3 Terminal condition setting of medium guidance correction trajectory

Missile	x_f/km	y_f/km	z_f/km	θ_f/(°)	ψ_{vf}/(°)
M1	600	20	37.07	0	0
M2	600	20	30	0	0
M3	600	27.07	30	0	0
M4	600	27.07	37.07	0	0

The simulation results are shown in Fig. 12 and Fig. 13. Fig. 12 and Fig. 13 show the simulation results of the four interceptors IIA covering the PIA of the target cooperatively. When the terminal capability of the interceptors is limited, the interceptors can only cover 2/3 of the PIA. When the target moves longitudinally in 30 s, the PIA changes from R_1 to R_2. According to the updated target PIA, the terminal position and velocity direction constraints of multiple interceptors are solved, and the trajectories are generated on-line as shown in Fig. 13. “stan traj” means standard trajectory, “cor traj” means correction trajectory. The revised trajectories enable the four interceptors IIA to cover the target PIA R_2 well, and the coverage rate can reach 0.91. The longitudinal adjustment ability of midcourse guidance and the effectiveness of the cooperative coverage of multiple interceptors are verified.

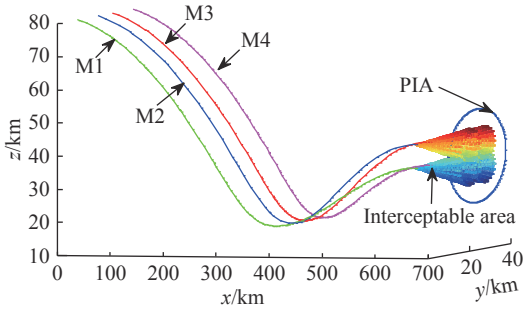

Fig. 12 Generation of four interceptors' standard trajectories

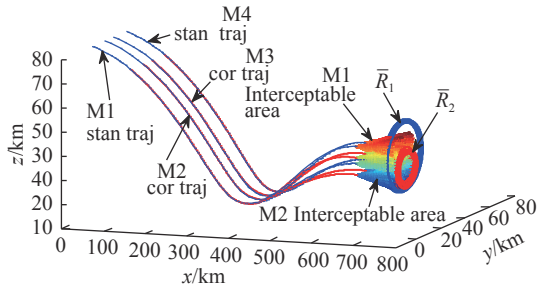

Fig. 13 Generation of four interceptors' correctional trajectories

Scenario 2: In order to verify the effectiveness of cooperative coverage after lateral adjustment of midcourse guidance trajectory of multiple interceptors, it is assumed that during midcourse guidance, the target measurement information has been updated four times in total, among which the projection of the PIA in the target encounter plane at the initial time of midcourse guidance is

$$\bar{R}_1 = \{(y,z)|-15\,000 \leqslant y \leqslant 65\,000,$$
$$30\,000 \leqslant z \leqslant 50\,000, \sigma_y = 13\,333, \sigma_z = 3\,333.3\}.$$

In the 10th second of midcourse guidance, the target measurement information is updated for the first time, and the PIA after updating is

$$\bar{R}_2 = \{(y,z)|1\,000 \leqslant y \leqslant 70\,000,$$
$$30\,500 \leqslant z \leqslant 49\,500, \sigma_y = 12\,405, \sigma_z = 2\,805.3\}.$$

In the 20th second of midcourse guidance, the target measurement information is updated for the second time, and the PIA after updating is

$$\bar{R}_3 = \{(y,z)|25\,000 \leqslant y \leqslant 82\,000,$$
$$32\,000 \leqslant z \leqslant 46\,500, \sigma_y = 9\,200, \sigma_z = 2\,100\}.$$

In the 30th second of midcourse guidance, the target measurement information is updated for the third time, and the PIA after updating is

$$\bar{R}_4 = \{(y,z)|45\,000 \leqslant y \leqslant 90\,000,$$
$$32\,500 \leqslant z \leqslant 44\,600, \sigma_y = 7\,200, \sigma_z = 1\,850\}.$$

In the 40th second of midcourse guidance, the measurement information of the target is updated for the fourth time, and the PIA is

$$\bar{R}_5 = \{(y,z)|56\,000 \leqslant y \leqslant 96\,000,$$
$$33\,600 \leqslant z \leqslant 43\,600, \sigma_y = 6\,666.7, \sigma_z = 1\,666.7\}.$$

According to the initial time of midcourse guidance, the PIA information at the hand-off time is obtained and generates four standard trajectories, the standard trajectories parameters are as follows in Table 4.

Table 4 Initial and terminal condition settings of medium guidance reference trajectory

V_0/(m/s)	x_0/km	z_0/km	θ_0/(°)	ψ_{v0}/(°)
3 000	0	80	−3	0
V_f/(m/s)	x_f/km	z_f/km	θ_f/(°)	ψ_{vf}/(°)
Max	600	40	0	0

Among them, M1, M2, M3 and M4 have the same position of the y-axis at the initial time and terminal time, which are 10 km, 20 km, 30 km, and 40 km. The trajectories have four corrections in terminal states as in Table 5.

Table 5 Terminal condition setting of medium guidance correction trajectory

Variable	Correction 1	Correction 2	Correction 3	Correction 4
dy_f /km	10	10	10	8
$d\psi_{vf}$/(°)	2	2	2	2

The simulation results are shown in Fig. 14 and Fig. 15.

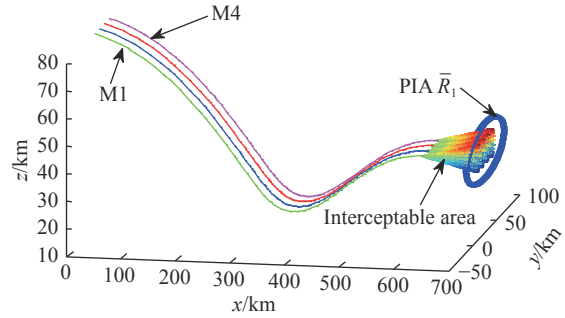

Fig. 14 Generation of four interceptors' standard trajectories

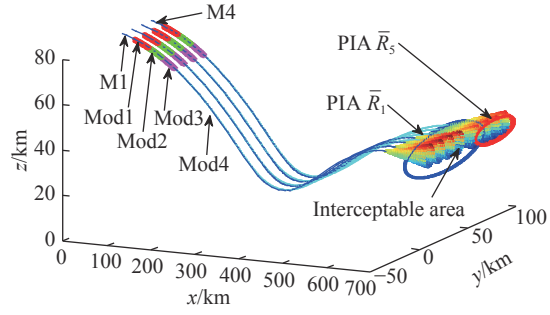

Fig. 15 Generation of four interceptors' correctional trajectories

Fig. 14 shows the standard trajectories generated offline by four interceptors, and the PIA in lateral is obviously more dispersive than that on the longitudinal direction. By optimizing the terminal state of the multiple interceptors, it is found that the multiple interceptors need to be deployed in the side intensively to achieve the maximum coverage of the PIA of the target in the IIA. It can be seen from Fig. 14 that the standard trajectories generated by interceptors can ensure the effective coverage of IIA to the PIA obtained at the initial time of midcourse guidance; with the continuous development of midcourse guidance of multiple interceptors, the PIA of targets has been updated four times, and the PIA obtained from the four updated target measurement information $\bar{R}_2$, $\bar{R}_3$, $\bar{R}_4$ and $\bar{R}_5$. According to the target PIA obtained at different times, calculate the terminal position and velocity direction constraints of multiple interceptors, and adjust the trajectories of multiple interceptors for four times, as shown in Fig. 15, Mod1−Mod4 mean four corrections in terminal states. Finally, ensure that the IIA of the four interceptors can cover the PIA $\bar{R}_5$ well, covering a probability integral of 0.89. It is verified that the ability of lateral continuous adjustment and the effectiveness of cooperative coverage of multiple interceptors are available.

5. Conclusions

Based on the method of on-line generation of midcourse guidance trajectory under neighborhood optimal control, through optimizing the zero control terminal position, this paper proposes a strategy of cooperatively covering the PIA. Aiming at the problem that the terminal guidance correction ability of a single interceptor is insufficient, the multiple interceptor area can be used to cover the target PIA. The hit probability of the interceptor is greatly increased.

References

[1] DWIVEDI P N, BHATTACHARYA A, PADHI R. Suboptimal midcourse guidance of interceptors for high-speed targets with alignment angle constraint. Journal of Guidance, Control, and Dynamics, 2011, 34(3): 860–877.

[2] HALBE O, RAJA R, PADHI R G. Robust reentry guidance of a reusable launch vehicle using model predictive static programming. Journal of Guidance, Control, and Dynamics, 2014, 37(1): 134–148.

[3] INDIG N, BEN-ASHER J Z, FARBER N. Near optimal spatial midcourse guidance law with angular constraint. Journal of Guidance, Control, and Dynamics, 2014, 37(1): 214–223.

[4] INDIG N, BEN-ASHER J Z, SIGAL E. Near-optimal minimum time guidance under a spatial angular constraint in atmospheric flight. Proc. of the AIAA Guidance, Navigation, and Control Conference, 2015: 5–9.

[5] PONTANI M, CECCHETTI G, TEOFILATTO P. Variable-time-domain neighboring optimal guidance, Part 1: algorithm structure. Journal of Optimal Theory Application, 2015, 166: 76–92.

[6] PONTANI M, CECCHETTI G, TEOFILATTO P. Variable-time-domain neighboring optimal guidance, Part 2: application to lunar decent and soft landing. Journal of Optimal Theory Application, 2015, 166: 93–114.

[7] PONTANI M, CECCHETTI G, TEOFILATTO P. Variable-time-domain neighboring optimal guidance applied to space trajectories. Acta Astronautica, 2015, 115: 102–120.

[8] HUI Y, FAHROO F, ROSS M I. Real-time computation of neighboring optimal control laws. Proc. of the AIAA Guidance, Navigation, and Control Conference and Exhibit, 2002: 1−7.

[9] TIAN B L, ZONG Q. Optimal guidance law for reentry vehicles based on indirect Legendre pseudospectral method. Acta Astronautica, 2011, 68(7/8): 1176–1184.

[10] WILLIAMS P. Application of pseudospectral methods for receding horizon control. Journal of Guidance, Engineering Notes, 2004, 27(2): 310–314.

[11] WU X Z. Guidance and control method of glider reentry. Beijing: Beijing University of Technology, 2015. (in Chinese)

[12] YANG L, ZHOU H, CHEN W C. Application of linear Gauss pseudospectral method in model predictive control. Acta Astronautica, 2014, 96: 175–187.

[13] ZHOU J, LEI H M, SHAO L, et al. Generation of optimal ballistic cluster for midcourse guidance of interceptors. Journal of National University of Defense Science and Technology, 2017, 39(5): 171–177. (in Chinese)

[14] ZHOU J, LEI H M, ZHAI D L, et al. Optimal midcourse trajectory cluster generation and trajectory modification for hypersonic interceptions. Journal of Systems Engineering and Electronics, 2017, 28(6): 1162–1173.

[15] LI N B, LEI H M, ZHOU J, et al. Variable-time-domain online neighboring optimal trajectory modification for hypersonic interceptors. International Journal of Aerospace Engineering, 2017, 2017: 9456179.

[16] LI N B, LEI H M, ZHOU J, et al. Design of tracking guidance law based on neighborhood optimal control. Journal of Beijing University of Technology, 2018, 38(1): 46–51. (in Chinese)

[17] LEI H M, LI N B, ZHOU J, et al. Optimal trajectory tracking guidance law of near space interceptor. Journal of National University of Defense Science and Technology, 2018, 40(1): 24–31. (in Chinese)

[18] LI N B, LEI H M, ZHOU J, et al. Design of midcourse guidance trajectory online optimization for near space interceptor. Control and Decision, 2017, 32(12): 2195–2200. (in Chinese)

[19] ZHAI C, HE F H, HONG Y G. Coverage-based interception algorithm of multiple interceptors against the target involving decoys. Journal of Guidance, Control, and Dynamics, 2016, 39(7): 1646–1652.

[20] DIONNE D, MICHALSKA H, RABBATH C A. Predictive guidance for pursuit-evasion engagements involving multiple decoys. Journal of Guidance, Control, and Dynamics, 2015, 30(5): 1277–1286.

[21] SU W S, LI K B, CHEN L. Coverage-based three-dimensional cooperative guidance strategy against high maneuvering target. Aerospace Science and Technology, 2019, 85: 556–566.

[22] MA L B, HE F H, YAO Y. A coverage-based guidance algorithm for the multiple-stage cooperative interception problem. Proc. of the 35th Chinese Control Conference, 2016.

DOI:10.1109/ChiCC.2016.7554641.

[23] WANG J W, HE F H, WANG L, et al. Cooperative guidance for multiple interceptors based on dynamic target coverage theory. Proc. of the 11th World Congress on Intelligent Control and Automation, 2014. DOI:10.1109/WCICA.2014.7053406.

[24] LIU X , LIANG X G. Integrated guidance and control of multiple interceptor missiles based on improved distributed cooperative control strategy. Journal of Aerospace Technology and Management, 2019. DOI:10.5028/jatm.v11.1003.

[25] WANG S J, WANG D C, YAN W Y, et al. Optimal system control. Beijing: Water Conservancy and Hydropower Press, 1985. (in Chinese)

[26] LEI H M, LI J, HU X J, et al. Theory of guidance and control for missile. Beijing: National Defense Industry Press, 2018. (in Chinese)

[27] BREAKWELL J V, SPEYER J L, BRYSON A E. Optimization and control of nonlinear systems using the second variation. SIAM Journal on Control and Optimization, 1963, 1(2): 193–223.

[28] BRYSON A E, HO Y C. Applied optimal control. New York: Halsted Press, 1975.

[29] Department of Applied Mathematics, Tongji University. Linear algebra. Beijing: Higher Education Press, 2006. (in Chinese)

[30] ZHAI D L, LEI H M, LI J, et al. Trajectory prediction of hypersonic vehicle based on adaptive IMM. Acta Aeronautica et Astronautica Sinica, 2016, 37(11): 3466–3475. (in Chinese)

Biographies

CHEN Wenyu was born in 1996. He is a doctoral degree candidate in the Air and Missile Defense College, Air Force Engineering University, Xi'an, China. His research interests are hypersonic vehicle controller design and hypersonic interception strategy.
E-mail: lorilouto_cwy@163.com

SHAO Lei was born in 1982. He is now an associate professor in the Air and Missile Defense College, Air Force Engineering University, Xi'an, China. His current research interests include advanced guidance law design, hypersonic vehicle controller design and hypersonic interception strategy.
E-mail: shaolei_zj@163.com

LEI Humin was born in 1960. He received his M.S. and Ph.D. degrees from Northwestern Polytechnical University, in 1989 and 1999 respectively. He is now a professor and a supervisor of doctors in the Air and Missile Defense College, Air Force Engineering University, Xi'an, China. His current research interests include advanced guidance law design, hypersonic vehicle controller design and hypersonic interception strategy.
E-mail: hmleinet@21cn.com